Cellular Physiology and Biochemistry

Cell Physiol Biochem 2018;51:2938-2954
DOI: 10.1159/000496045
Published online: 14 December 2018
Accepted: 6 December 2018

Original Paper

Sinoporphyrin Sodium-Mediated Sonodynamic Therapy Inhibits RIP3 Expression and Induces Apoptosis in the H446 Small Cell Lung Cancer Cell Line

Jing Shen[a] Shoubo Cao[a] Xin Sun[b] Bo Pan[a] Jingyan Cao[a] Dehai Che[a] Shi Jin[a] Yingyue Cao[a] Ye Tian[b] Yan Yu[a]

[a]Department of Medical Oncology, Harbin Medical University Cancer Hospital, Harbin, [b]Department of Cardiology, the First Affiliated Hospital, Cardiovascular Institute, Harbin Medical University, Harbin, China

Key Words
H446 cells • Sinoporphyrin sodium • Sonodynamic therapy • Apoptosis • Reactive oxygen species

Abstract
Background/Aims: Sonodynamic therapy (SDT) is expected to be a new method to solve the clinical problems caused by advanced metastasis in patients with lung cancer. The use of ultrasound has the advantage of being noninvasive, with deep-penetration properties. This study explored the anti-tumor effect of SDT with a new sonosensitizer, sinoporphyrin sodium (DVDMS), on the human small cell lung cancer H446 cell line *in vitro* and *in vivo*. ***Methods:*** Absorption of DVDMS was detected by a fluorescence spectrophotometer, and DVDMS toxicity was determined using a Cell Counting Kit-8. Mitochondrial membrane potential (MMP) was assessed using the JC-1 fluorescent probe. Cell apoptosis was measured by flow cytometry, and apoptosis-related proteins were detected by western blotting. The expression of cytokines was measured using an enzyme-linked immunosorbent assay and quantitative real-time PCR. To verify the *in vitro* results, we detected tumor volumes and weight changes in a xenograft nude mouse model after DVDMS-SDT. Hematoxylin and eosin staining was used to observe changes to the tumor, heart, liver, spleen, lung, and kidney of the mice, and immunohistochemistry was used to examine changes in the expression of tumor CD34 and receptor-interacting protein kinase-3 (RIP3), while terminal deoxynucleotidyl transferase-mediated dUTP nick-end labeling was used to observe apoptosis in tumor tissues. ***Results:*** DVDMS-SDT-treated H446 cells increased the rate of cellular apoptosis and the levels of reactive oxygen species (ROS), cleaved caspase-3, cleaved caspase-8, cleaved caspase-9, and caspase-10, and decreased the levels of MMP, RIP3, B-cell lymphoma 2, vascular endothelial growth factor, and tumor necrosis factor-α. The sonotoxic effect was mediated by ROS and

Jing Shen and Shoubo Cao contributed equally to this work.

Prof. Yan Yu
Department of Medical Oncology, Harbin Medical University Cancer Hospital
No. 150 Haping Road, Harbin, 150081 (China)
Tel. +86-451-86298727, Fax +86-451-86298727, E-Mail yuyan@ems.hrbmu.edu.cn

was reduced by a ROS scavenger (N-acetyl-L-cysteine). In the *in vivo* mouse xenograft model, DVDMS-SDT showed efficient anti-cancer effects with no visible side effects. ***Conclusion:*** DVDMS-SDT induced apoptosis in H446 cells, in part by targeting mitochondria through the mitochondria-mediated apoptosis signaling pathway, and the extrinsic apoptosis pathway was also shown to be involved. Both apoptosis and changes in RIP3 expression were closely related to the generation of ROS. DVDMS-SDT will be advantageous for the management of small cell lung cancer due to its noninvasive characteristics.

Introduction

Lung cancer remains the leading cause of cancer-related mortality. Invasion and migration are significant biological characteristics of lung cancer. Small cell lung cancer (SCLC) represents approximately 15% of all cases [1]; most patients with SCLC are diagnosed at an advanced stage, and limited treatment strategies can be applied to these patients, resulting in a poor prognosis, with a 5-year survival rate of less than 10% [1]. Radiotherapy and chemotherapy are traditional treatments for SCLC; however, patients may discontinue treatment due to the presence of serious adverse effects [2]. In addition, in patients with recurrence and treatment failure, there are even less available therapeutic strategies. Thus, novel noninvasive and safe strategies with limited toxicity are urgently needed.

Photodynamic therapy (PDT) has emerged as an alternative to conventional chemo- and radiation-based therapies in the treatment of certain cancers such as skin, head and neck, and prostate cancer [3-7]. However, PDT has significant shortcomings. Firstly, the penetration of light into deep tumor tissues is limited, which is essential for the activation of the photosensitizer. Secondly, certain potential side effects are serious, such as long-lasting skin sensitivity due to the continuous retention of the photosensitizer in cutaneous tissues [2, 8]. Sonodynamic therapy (SDT), which consists of ultrasound and a sonosensitizer, has been studied widely *in vitro* and *in vivo* [2, 8-13]. SDT has an advantage over PDT in that it can penetrate deep tumor tissues, making it applicable to a wide range of cancers.

The scientific basis of SDT relies on the generation of reactive oxygen species (ROS) through the simultaneous combination of low intensity ultrasound, molecular oxygen, and a sensitizing drug [14]. Recently, a novel sensitizer (sinoporphyrin sodium, referred to as DVDMS) was granted independent intellectual property status in China [15]. This sensitizer shows higher photochemical activity than porfimer sodium (Photofrin), which has been approved by the Food and Drug Administration of the USA for use as a sensitizer in PDT for cancer. In some experiments, it was found that SDT could influence gene expression to induce apoptosis [16]. Many investigators believe that apoptosis plays a vital role in the anti-cancer effect of SDT. Oxidative stress has also been recognized to play a pivotal role in the process of SDT-induced apoptosis and cytotoxicity. However, the underlying mechanism governing the regulation of intracellular ROS generation and cell apoptosis in SDT remains undefined.

"Programmed" or "regulated" necrotic cell death is described as necroptosis, which is distinguished from its counterpart, apoptosis, in that caspase activation is dispensable for cell death, and, unlike apoptosis, necroptosis results in plasma membrane rupture, thus releasing the contents of the cell and triggering activation of the immune system [17]. Receptor-interacting protein kinase-3 (RIP3 or RIPK3), a Ser/Thr kinase that belongs to the RIP kinase family, is an essential part of the cellular machinery that executes necroptosis [18]. The activation of necroptosis includes the formation of a complex containing RIP3 and RIP1 (or RIPK1) and the recruitment of mixed lineage kinase domain-like protein [19]. However, the effect of necroptosis in the anti-tumor action of SDT remains largely unclear.

In this study, we explored the anti-tumor effect of SDT with the novel porphyrin-derived sonosensitizer DVDMS, *in vitro* and *in vivo*, using the human SCLC H446 cell line and a mouse SCLC xenograft model. We aimed to determine whether manipulation of ultrasonic intensity would influence the SDT-induced elevation of ROS generation and RIP3 expression and the type of cell death involved.

Materials and Methods

Sensitizer

DVDMS (with a purity of 98.5%) was a gift from Dr. Ye Tian (Department of Cardiology, the First Affiliated Hospital of Harbin Medical University). It was dissolved in phosphate-buffered saline (PBS; g/L: NaCl 8.0 g, KCl 0.2 g, Na_2HPO_4 1.44 g, KH_2PO_4 0.24 g, pH 7.2) at a storage concentration of 1 mg/mL, and was stored in the dark at –20°C.

Cell culture

The H446 cell line, human lung adenocarcinoma A549 cell line, and lung squamous carcinoma H520 cell line were purchased from the American Type Cell Collection (Manassas, VA). Cells were cultured in RPMI 1640 medium (Gibco, Carlsbad, CA) supplemented with 10% fetal calf serum. The cells were maintained using an EGM-2 Bullet Kit (Lonza, Basel, Switzerland) in a humidified atmosphere of 5% CO_2 at 37°C. The inhibitors Ac-DEVD-CHO and Z-VAD-FMK were obtained from the Beyotime Institute of Biotechnology (Jiangsu, China) and used at appropriate concentrations (both at 20 μM).

Animals

Animal experiments were performed in accordance with the National Institutes of Health Guide for the Care and Use of Laboratory Animals and were approved by the Institutional Animal Care and Use Committee of Harbin Medical University. BALB/c nude mice (female, 4–5 weeks old) were obtained from VITAL RIVER (Beijing, China). Mice were housed at room temperature with free access to food and water. After a 1-week acclimation period, the mice were subcutaneously injected into their backs with 0.2 mL of H446 cells (1.0×10^7cells/mL). When the tumors reached an average diameter of 2–4 mm, the tumor-bearing mice were assigned randomly to different groups. Tumor growth was measured every 3 days. The longest (a) and shortest (b) diameters of the tumor were determined with a caliper, and tumor volume (V) was calculated as: $V = (a \times b^2)/2$.

Histological examination by hematoxylin and eosin staining

Xenograft tumor tissues and main organs (heart, liver, spleen, lung, and kidney) from the different groups were fixed in 10% buffered formalin for 24 h and then embedded in paraffin. The samples were sliced into 5-μm-thick sections and stained with hematoxylin and eosin (H&E). Histopathological changes in each group were observed under a light microscope.

SDT

The SDT equipment used in this study, including an ultrasonic generator, transducer, and power amplifier, was assembled by the Harbin Institute of Technology (Harbin, China). A homemade ultrasonic transducer (diameter: 3.5 cm; resonance frequency: 0.5 MHz; duty factor: 10%; repetition frequency: 100 Hz) was placed in a water bath at 30 cm below the cells. Ultrasonic intensity was set at 0.5 W/cm^2, as measured by a hydrophone (Onda Corp., Sunnyvale, CA). Cell lines (0.5×10^6 cells/mL) were seeded in 35-mm culture dishes, consistent with the size of the therapeutic instrument probe, before SDT. Cells were incubated with 4 μmol/L DVDMS (Sigma-Aldrich, St. Louis, MO) in the dark for 4 h prior to treatment with the SDT equipment.

The *in vivo* experimental apparatus for ultrasound was similar to that used *in vitro*. A focused ultrasound transducer with a frequency of 1.1 MHz was submerged in degassed water in a tank facing directly upward. When the tumors grew to approximately 2–4 mm in diameter (approximately 6 days after injection), the animals were divided randomly into five groups: control (control), 2 mg/kg DVDMS solution alone (DVDMS), ultrasound alone once (US), DVDMS-SDT once (SDT1), and DVDMS-SDT twice (SDT2). Ultrasound radiation was applied for 5 min at each treatment. Injections were performed into the caudal vein after DVDMS administration (4 h). All experiments were performed in the dark to avoid excitation of DVDMS.

Cellular uptake of DVDMS

To determine intracellular DVDMS levels, the cells were collected after different incubation periods (0, 1, 2, 3, 4, 5, and 6 h) and examined using a fluorospectrophotometer (HORIBA Scientific, Piscataway, NJ) and a fluorescence microscope (Zeiss, Oberkochen, Germany). The mean fluorescence intensity of DVDMS was recorded under the same measurement conditions.

Detection of intracellular ROS

Intracellular ROS were detected by means of an oxidation-sensitive fluorescent probe (DCFH-DA; Beyotime Institute of Biotechnology). After treatment with or without 10 mmol/L N-acetyl-L-cysteine (NAC; Invitrogen, Carlsbad, CA) for 0–12 h, the cells were washed twice with PBS. They were then incubated with 10 μmol/L DCFH-DA at 37ºC for 20 min according to the manufacturer's instructions.

Cell apoptosis assay

Apoptosis in H446 cells was measured by flow cytometry with an Annexin V-FITC Apoptosis Detection Kit (Beyotime Institute of Biotechnology) according to the manufacturer's instructions. Briefly, after isolation or incubation, H446 cells were washed twice with ice-cold PBS and then resuspended in binding buffer. Cells were analyzed by flow cytometry within 10 min of annexin V-propidium iodide (PI) labeling. Fluorescence parameters were gated using unstained and single-stained untreated cells. Viable H446 cells were defined as negative for annexin V-FITC and PI staining, and total apoptosis was expressed as the percentage of annexin V-positive plus annexin V and PI double-positive cells minus background fluorescence. At least 10, 000 stained cells were analyzed on a FACS Caliber system (Becton Dickinson, Bedford, MA) for each determination. Data were analyzed using Cell Quest software (Becton Dickinson, Bedford, MA).

Quantitative real-time PCR analysis

Total RNA from cultured cells was extracted after treatment using the TRIzol reagent (Invitrogen) according to the manufacturer's protocol. Complementary DNA was synthesized from 500 ng total RNA using a PrimeScript™ RT Reagent Kit with DNA Eraser (Takara Bio, Inc., Dalian, China) in a final reaction volume of 20 μL. Quantitative real-time PCR (qRT-PCR) was performed using SYBR Green Master Mix (Roche Applied Science, Mannheim, Germany) on an ABI7500 Sequence Detection System (Applied Biosystems, Foster City, CA). Glyceraldehyde 3-phosphate dehydrogenase (GAPDH) was used as the internal control to correct for variations in cDNA content among the samples. The primers are shown in Table 1 and were synthesized by Oligofectamine (Takara Bio). No amplification of nonspecific products was observed in any of the reactions, as determined from an analysis of the dissociation curves. Data were normalized to GAPDH expression levels and are presented as the averages from three repeated experiments. Relative gene expression levels were calculated using the comparative Ct (△△Ct) method; relative expression is calculated as $2^{-\triangle\triangle Ct}$, where Ct represents the threshold cycle.

Western blot analysis

Total protein extracts were prepared from cells by homogenization in lysis buffer containing a protease inhibitor cocktail (Complete; Roche Applied Science) and phosphatase inhibitor (Roche Applied Science). The lysates were centrifuged at 15, 000 × *g* for 15 min at 4°C. Protein concentrations in the lysates were determined using a protein analyzer (SmartSpec 3000 Spectrophotometer; Bio-Rad Laboratories, Hercules, CA) according to the manufacturer's protocol. Protein samples (50 μg) from the different groups were boiled for 5 min in sample buffer, separated by 10% sodium dodecyl sulfate-polyacrylamide gel electrophoresis, and transferred onto a nitrocellulose membrane (Bio-Rad Laboratories). Nonspecific reactivity was blocked in 5% nonfat dry milk in TBST (10 mM Tris-HCl, pH 7.5, 150 mM NaCl, 0.05% Tween-20) for 1 h at room temperature. The membrane was then incubated with primary antibodies against RIP-3 (1:200; Cell Signaling Technology, Danvers, MA), protein kinase B (also known as AKT;

Table 1. Primers for qRT-PCR

Enzymes	Forward (5′–3′)	Reverse (5′–3′)
TGF-β	GATGTCACCGGAGTTGTGC	TGCAGTGTGTTATCCCTGCT
IL-6	TACATCCTCGACGGCATCTC	CCATCTTTGGAAGGTTCAGG
VEGF	TCCTCACACCATTGAAACCA	ATCCTGCCCTGTCTCTCTGT
TNF-α	GCTGGTTATCTCTCAGCTCCA	AAGCCTGTAGCCCATGTTGT
RIP3	TGGTTCTCCTAAAGCCATCC	ATGAATGCTGCTGTCTCCAC
GAPDH	AGAAGGCTGGGGCTCATTTG	AGGGGCCATCCACAGTCTTC

1:500; Cell Signaling Technology), p-AKT (1:200; Cell Signaling Technology), signal transducer and activator of transcription (STAT3; 1:500; Cell Signaling Technology), p-STAT3 (1:500; Cell Signaling Technology), mitogen-activated protein kinase (MAPK; 1:500; Millipore, Bedford, MA), B-cell lymphoma 2 (BCL-2; 1:200; Cell Signaling Technology), cleaved caspase-3 (1:200; Cell Signaling Technology), cleaved caspase-8 (1:500; Beyotime Institute of Biotechnology), cleaved caspase-9 (1:500; Beyotime Institute of Biotechnology), caspase-8 (1:200; Boster Biological Technology, Wuhan, China), and GAPDH (1:1000; Beyotime Institute of Biotechnology) in the same solution overnight at 4°C. The blot was rinsed and incubated with a horseradish peroxidase-conjugated secondary antibody (1:2000; Zhongshan Golden Bridge Biotechnology Co., Beijing, China) at 37°C for 1 h. Protein bands were visualized using an electrochemiluminescence kit (TransGen Biotechnology Co., Ltd., Beijing, China) and captured with a scanner (V30; Epson, Tokyo, Japan). Data were quantified using Quantity One Version 4.6.2 (Bio-Rad Laboratories).

Mitochondrial membrane potential assessment

Mitochondrial membrane potential (MMP) was assessed using the JC-1 fluorescent probe (Beyotime Institute of Biotechnology) according to the manufacturer's instructions. Briefly, seeded cells (2.0×10^5 cells/mL) were pre-treated with the indicated concentrations of test compounds for 1 h and exposed to ultrasound. At 4 h after DVDMS-SDT, H446 cells were incubated with 10 mg/mL JC-1 for 20 min at 37°C in the dark and measured by a multimode microplate reader at 525 nm excitation and 590 nm emission wavelengths for aggregates and at 490 nm excitation and 530 nm emission for monomers. The cells were then photographed under a fluorescence microscope.

Enzyme-linked immunosorbent assay

Angiogenic factor concentrations were determined using a commercial enzyme-linked immunosorbent assay (ELISA) kit (USCN Life Science, Houston, TX) according to the manufacturer's instructions.

Terminal deoxynucleotidyl transferase-mediated dUTP nick-end labeling assay for apoptotic cells in vivo

Paraffin-embedded SCLC xenograft samples were stained with a terminal deoxynucleotidyl transferasemediated dUTP nick-end labeling (TUNEL) assay kit (Roche Applied Science) according to the manufacturer's instructions. Under a fluorescence microscope, apoptotic cells exhibited yellow-green fluorescence in the nucleus after excitation with blue light. DAPI was used to stain nuclei.

Immunohistochemistry

Paraffin-embedded tumor tissue sections were dewaxed, rehydrated, and heated for antigen retrieval in 0.01 mmol/L citrate buffer (pH 6.0). The sections were immersed in a 3% hydrogen peroxide solution for 10 min to block endogenous peroxidase activity. The sections were incubated with a rabbit monoclonal anti-CD34 antibody (Abcam, Cambridge, UK) and rabbit polyclonal anti-RIP3 antibody (GeneTex, Irvine, CA) overnight at 4°C. After washing, the sections were incubated with a secondary antibody for 20 min at room temperature. Finally, the sections were visualized with 3, 3′-diaminobenzidine and counterstained with hematoxylin solution.

Statistical analysis

Statistical analysis was performed with SPSS 17.0 software (SPSS Inc., Chicago, IL). Each treatment was performed in duplicate and the experiments were repeated independently three times. Measurement values are expressed as the mean ± standard deviation (SD). One-way analysis of variance (ANOVA) followed by the Student-Newman-Keuls (SNK) test were used to determine differences among the groups. Repeated-measures ANOVA was used to analyze body weight and tumor volume among the groups. Differences with $P < 0.05$ were considered statistically significant.

Results

Cellular uptake of DVDMS

The optimum uptake of DVDMS by three different lung cancer cell lines was investigated prior to ultrasonic irradiation. The uptake kinetics were determined by measuring the cellular fluorescence signal using fluorospectrophotometry and fluorescence microscopy. We found that the absorption of DVDMS by the three cell lines increased with time, peaked at 3 h, and was followed by a slow decline (Fig. 1A). The fluorescence signal of DVDMS elevated gradually and reached a maximum at approximately 3–4 h with a DVDMS concentration of 4 μg/mL in H446 cells (Fig. 1B). In the following experiments, we chose 3 h as the incubation time of cells with DVDMS.

Induction of apoptosis in H446 cells after DVDMS-SDT

To dissect the functional roles of DVDMS-SDT in cytotoxicity, cell survival was quantified using a Cell Counting Kit-8 (CCK-8) and flow cytometry. The viability of H520, A549, and H446 cells under different DVDMS concentrations was detected by CCK-8 assays. As shown in Fig. 2B, there was no significant difference in cell viability. According to a combination of previous reports [11, 20], we choose 4 μg/mL as the concentration of DVDMS. The

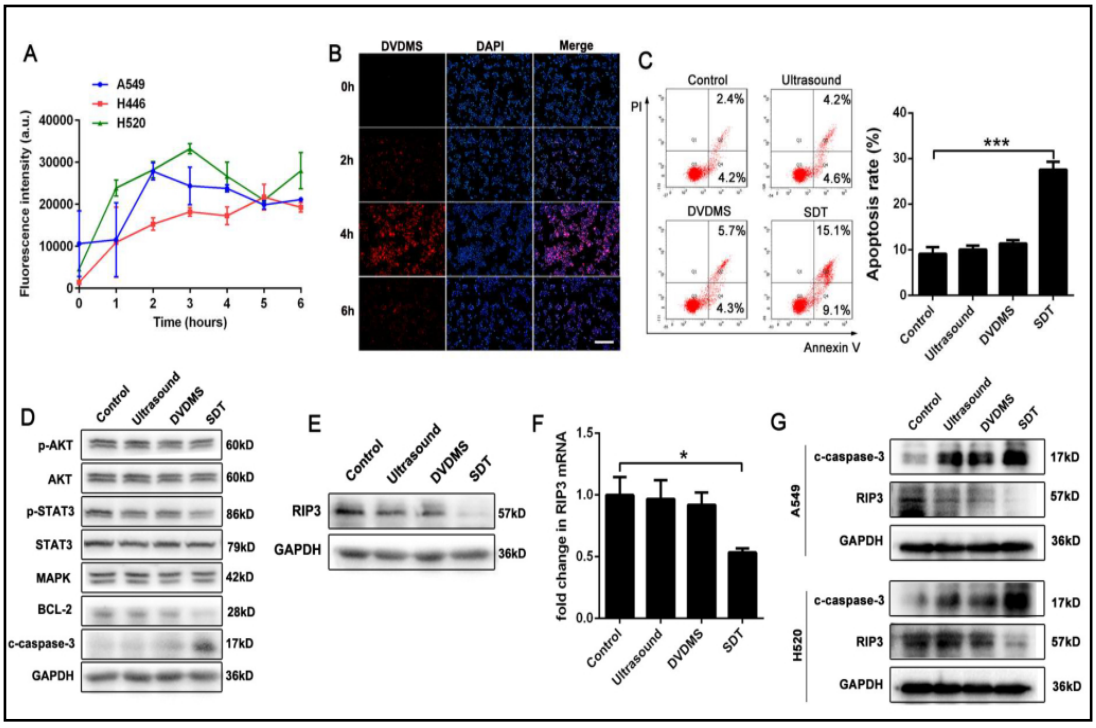

Fig. 1. Induction of apoptosis by DVDMS-SDT. (A) The uptake kinetics of 4 μg/mL DVDMS were determined by measuring cellular fluorescence using a fluorospectrophotometer in H520, A549, and H446 cells for 0–6 h. The data shown represent the mean ± SD. (B) H446 cells were incubated in 4 μg/mL DVDMS for 0, 2, 4, and 6 h. DVDMS uptake was detected by fluorescence microscopy. Scale bar represents 0.1 mm. (C) Apoptotic cells were detected by flow cytometry. H446 cells were stained with annexin V-FITC and PI. The number in each quadrant indicates the proportion of cells that are present in the quadrant. The bar graph depicts the apoptotic rate as the percentage of cells in the lower-right (annexin-V+/PI−) and upper-right (annexin-V+/PI+) quadrants. The data shown represent the mean ± SD and were analyzed by ANOVA followed by the SNK test. ***P<0.001. (D) Immunoreactive bands for p-AKT, AKT, p-STAT3, STAT3, MAPK, BCL-2, and c-caspase-3. (E and F) Western blot and qRT-PCR analyses of RIP3 expression in H446 cells. Data shown represent the mean ± SD and were analyzed by ANOVA followed by the SNK test. *P<0.05. (G) Western blot analysis of c-caspase-3 and RIP3 protein levels in A549 and H520 cells.

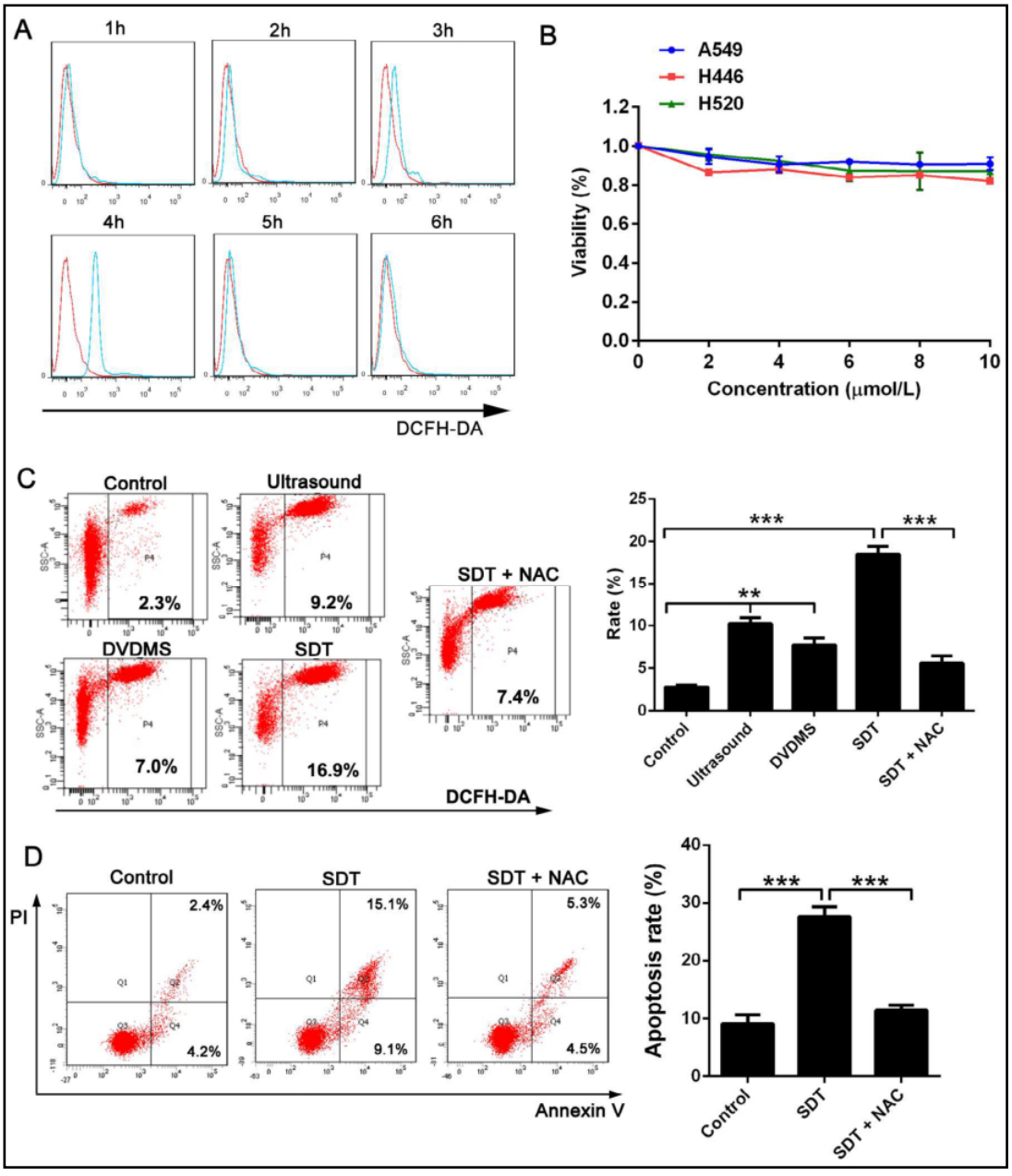

Fig. 2. ROS play a key role in DVDMS-SDT-induced apoptosis in H446 cells. (A) ROS generation in H446 cells after DVDMS-SDT at different time points. Flow cytometry analysis of ROS levels using a DCFH-DA probe. (B) Viability of H520, A549, and H446 cells under different concentrations of DVDMS was detected by CCK-8 assays. The data shown represent the mean ± SD. (C) Flow cytometry analysis of ROS levels in H446 cells. The data shown represent the mean ± SD and were analyzed by ANOVA followed by the SNK test. **P<0.01, ***P<0.001. (D) Apoptotic cells were detected by flow cytometry. The bar graph depicts the apoptotic rate as the percentage of cells in the lower-right (annexin-V+/PI−) and upper-right (annexin-V+/PI+) quadrants. Data shown represent the mean ± SD and were analyzed by ANOVA followed by the SNK test. ***P<0.001.

apoptotic cells were stained with annexin V-FITC and PI. Annexin V bound to the cells early in apoptosis, and continued to be bound through to cell death. PI was distinguished in the later stages of cell apoptosis or in already dead cells. At 6 h after DVDMS-SDT, H446 cells showed a markedly increased cell apoptosis rate (early and late stages) (Fig. 1C) compared with the control, US, and DVDMS groups.

DVDMS-SDT inhibits the expression of RIP3 and induces caspase activation

To explore further the mechanism underlying the induction of apoptosis by DVDMS-SDT, we analyzed the activation of cell signaling proteins in H446 cells by western blotting. AKT is a serine-threonine protein kinase that is critical for transmitting growth-promoting signals during the regulation of apoptosis [21]. STAT3 is a transcription factor that is activated in response to ligands such as interferons, epidermal growth factor, interleukin (IL)-5, and IL-6. STAT3 mediates the expression of a variety of genes in response to cell stimuli, and thus plays a key role in many cellular processes such as cell growth and apoptosis [22]. MAPKs act as an integration point for multiple biochemical signals and are involved in a wide variety of cellular processes such as proliferation, differentiation, transcription regulation, inflammation, and apoptosis. BCL-2 and caspase-3 are mitochondrial apoptosis regulatory factors [23]. The above proteins were expressed in the cytoplasm of each group (Fig. 1D). The expression of cleaved caspase-3 (c-caspase-3) was higher in the DVDMS-SDT group than in the control group, while the expression of BCL-2 and p-STAT3 was lower (Fig. 1D).

Surprisingly, it was observed that DVDMS-SDT led to a significant decline of RIP3 protein levels. The expression of RIP3 mRNA in H446 cells treated with DVDMS-SDT was evaluated by qRT-PCR using GAPDH mRNA as an internal reference for normalization. Compared with control cells, RIP3 mRNA expression was significantly decreased by 0.5-fold in the DVDMS-SDT group (Fig. 1E and 1F). We next investigated the activation of caspase-3 in the H520 and A549 cell lines. DVDMS-SDT increased the expression of c-caspase-3 and decreased RIP3 protein levels compared with the other groups in H520 and A549 cell lines (Fig. 1G).

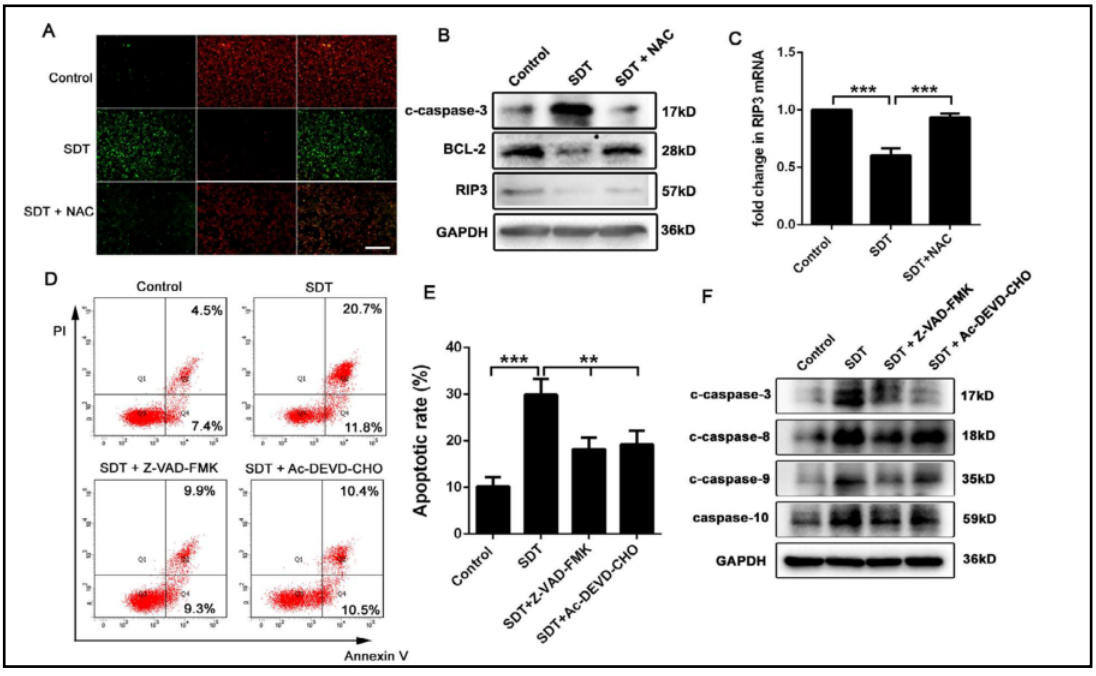

Fig. 3. DVDMS-SDT activates caspases in H446 cells. (A) Representative photographs of the effects of the test compounds on the DVDMS-SDT-induced loss of MMP using JC-1 by fluorescence microscopy. Scale bar represents 0.1 mm. (B) Immunoreactive bands for BCL-2, c-caspase-3, and RIP3. (C) qRT-PCR of RIP3 expression levels in H446 cells. The data shown represent the mean ± SD and were analyzed by ANOVA followed by the SNK test. ***P<0.001. (D) Apoptotic cells were detected by flow cytometry. (E) The bar graph depicts the apoptotic rate as the percentage of cells in the lower-right (annexin-V+/PI−) and upper-right (annexin-V+/PI+) quadrants. Data shown represent the mean ± SD and were analyzed by ANOVA followed by the SNK test. **P<0.01, ***P<0.001. (F) Immunoreactive bands for c-caspase-3, c-caspase-8, c-caspase-9, and caspase-10.

ROS play a key role in DVDMS-SDT-induced apoptosis in H446 cells

To examine further whether increased oxidative stress is associated with DVDMS-SDT-induced apoptosis in H446 cells, we detected the generation of ROS by using the specific probe DCFH-DA. We found that ROS levels were increased with time after DVDMS-SDT, and reached a maximum at approximately 3–4 h, which was followed by a slow decline until 6 h (Fig. 2A). DVDMS-SDT indeed increased intracellular ROS generation and the relative level of ROS abolished by pre-treatment with NAC (Fig. 2C). The apoptosis in H446 cells induced by DVDMS-SDT was inhibited by NAC (Fig. 2D). These observations provided compelling evidence to support our emerging view that oxidative stress acts as an integration point in the DVDMS-SDT-triggered apoptosis pathway.

DVDMS-SDT activates caspases by ROS generation

During the process of apoptosis, MMP dissipates. We detected MMP using JC-1. Most DVDMS-SDT-treated H446 cells displayed green fluorescence and lower MMP, while cells pre-treated with NAC presented with red-orange fluorescence due to the reversion of MMP loss. In line with this, the ratio of the red/green fluorescence intensity of JC-1 was notably recovered in the DVDMS-SDT+NAC group in comparison with the DVDMS-SDT group (Fig. 3A). Similarly, pre-incubation with NAC also prevented the DVDMS-SDT-induced increase of c-caspase-3 and decrease in RIP3 and BCL-2 expression (Fig. 3B). The mRNA level of RIP3 was decreased by DVDMS-SDT, but this decrease was abrogated by NAC (Fig. 3C). Next, we investigated the effects of DVDMS-SDT on the activation of caspases in H446 cells. DVDMS-SDT increased the levels of c-caspase-3, c-caspase-8, c-caspase-9, and caspase-10. We used a commercially available pan-caspase inhibitor, Z-VAD-FMK, to pharmacologically block caspase activity, and a caspase-3-specific inhibitor, Ac-DEVD-CHO, was used to block caspase-3 activity. Z-VAD-FMK dramatically inhibited the DVDMS-SDT-induced increase of c-caspase-3, c-caspase-8, c-caspase-9, and caspase-10. While DVDMS-SDT induced the activation of caspase-3, this was inhibited by Ac-DEVD-CHO (Fig. 3F). Meanwhile, we found that the DVDMS-SDT-induced apoptosis of H446 cells was inhibited by Z-VAD-FMK and Ac-DEVD-CHO (Fig. 3D and 3E).

DVDMS-SDT changes cytokine expression in H446 cells

Consistent with the changes in apoptosis and cell signaling proteins, H446 cells treated with DVDMS-SDT significantly decreased the expression of tumor-promoting cytokines compared to control cells. Vascular endothelial growth factor (VEGF) is a signaling protein produced by cells that stimulates the formation of blood vessels. When VEGF is overexpressed, it can contribute to disease. Solid cancers cannot grow beyond a limited size without an adequate blood supply; cancers that express VEGF are able to grow and metastasize [24]. Tumor necrosis factor (TNF)-α is a monocyte-derived cytotoxin that has been implicated in septic shock and cachexia [25]. ELISA and qRT-PCR were used to detect the expression of cytokines. We found that DVDMS-SDT selectively down-regulated TNF-α and VEGF protein expression in H446 cells (Fig. 4B); we also observed a similar increase in their mRNA levels (Fig. 4A). The most prominent decrease in secretion was for VEGF, with a 3-fold decrease, followed by TNF-α (0.2-fold decrease). By contrast, the production of IL-6 and transforming growth factor (TGF)-β by H446 cells was not significantly affected by DVDMS-SDT. NAC dramatically inhibited the DVDMS-SDT-decreased expression of VEGF and TNF-α.

Tumor growth is significantly inhibited by DVDMS-SDT

We used an H446 xenograft mouse model to investigate the effect of US combined with DVDMS on tumor growth. Due to the difficulty of detecting DVDMS in animal tissues, the pharmacokinetics of this agent after intravenous administration to mice could not be assessed in this study. Instead, the time course of sonication for up to 4 h after DVDMS administration was evaluated preliminarily by assessing its inhibitory effects on tumor cell growth. When the diameter of the tumors was at 2–4 mm, the mice were divided randomly into five groups: normal control group (control), ultrasound alone group (US), DVDMS alone

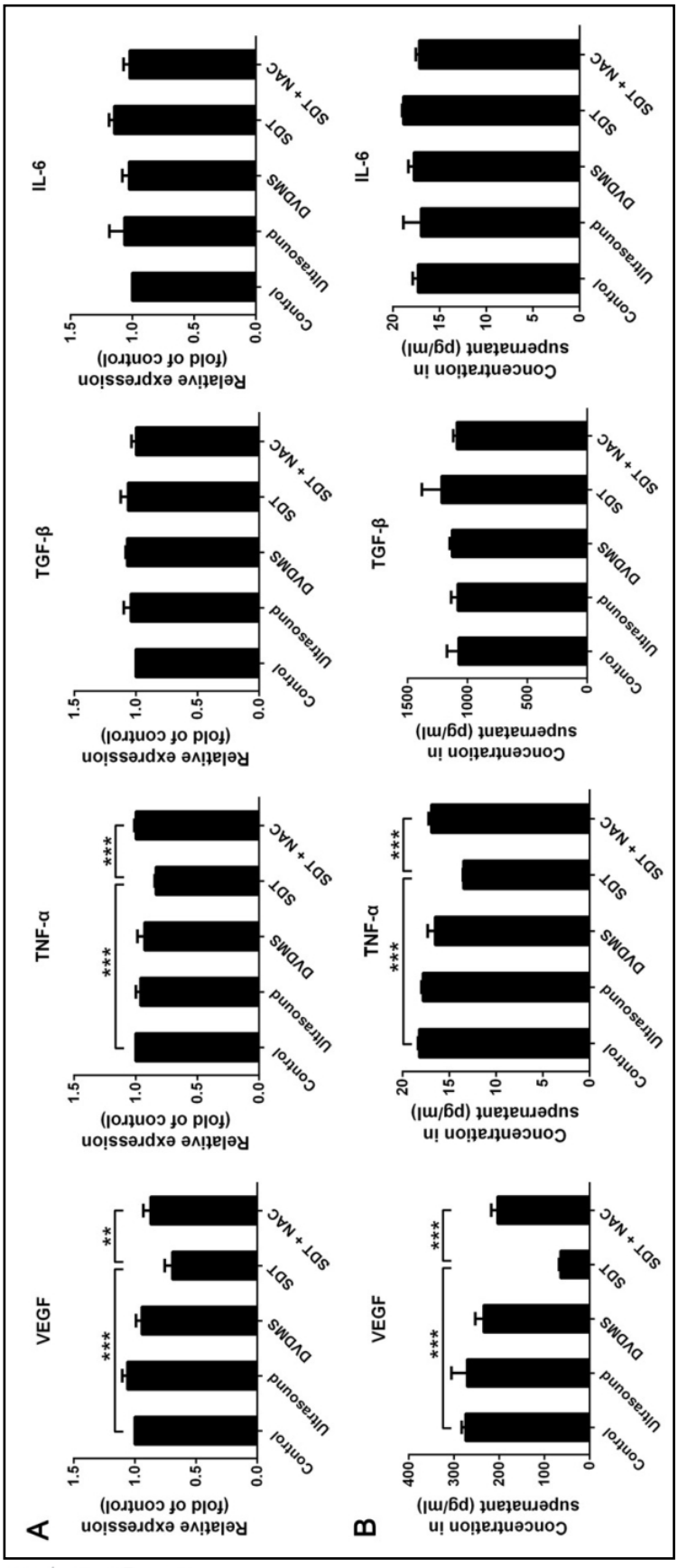

Fig. 4. DVDMS-SDT changes cytokine expression in H446 cells. (A) qRT-PCR of VEGF, TNF-α, TGF-β, and IL-6 mRNA levels. Data shown represent the mean ± SD and were analyzed by ANOVA followed by the SNK test. **P<0.01, ***P<0.001. (B) ELISA-determined protein levels of VEGF, TNF-α, TGF-β, and IL-6. Data shown represent the mean ± SD and were analyzed by ANOVA followed by the SNK test. ***P<0.001.

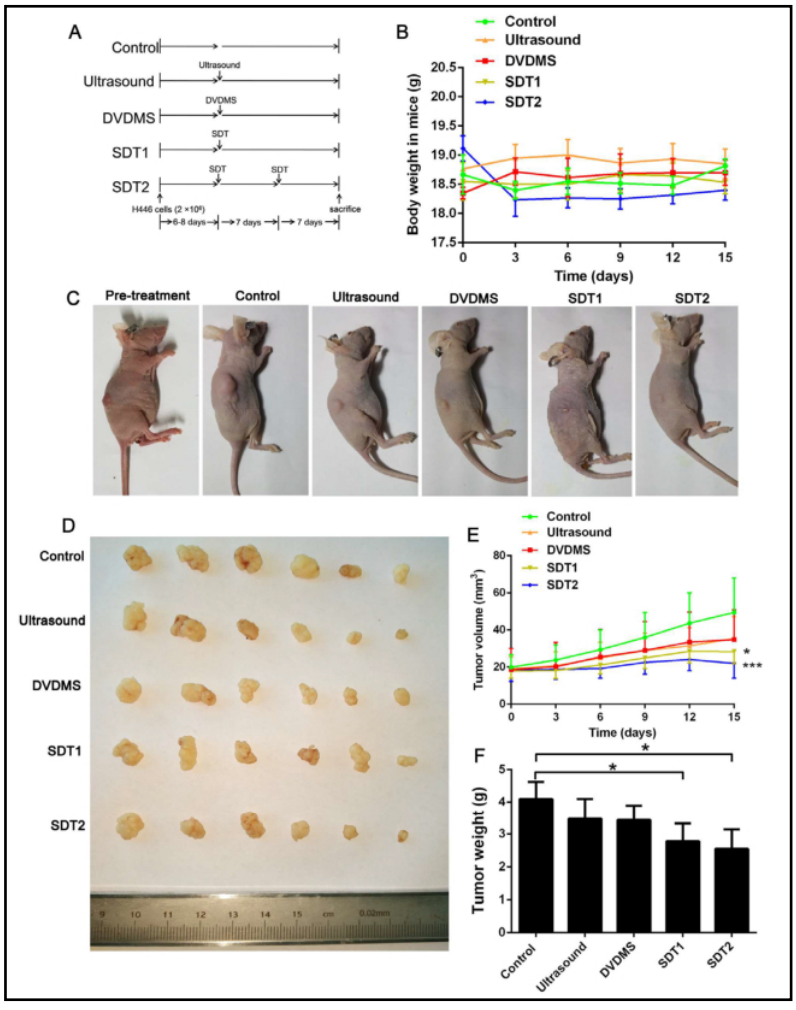

Fig. 5. Tumor growth is significantly inhibited by DVDMS-SDT. (A) Schema of the treatment schedule. (B) Body weight of mice from each group in the observation period. Data shown represent the mean ± SD. (C) Typical photographs of mice at the end of the experiment, after inoculation with H446 cells from each group. (D) Gross morphology of tumors excised from each group of mice at 15 days after treatment. (E) Development of tumor volume after various treatments. Data shown represent the mean ± SD and were analyzed by repeated-measures ANOVA. *P<0.05, ***P<0.001. (F) Tumor weight in each group on the 15th day after treatment. Data shown represent the mean ± SD and were analyzed by ANOVA followed by the SNK test. *P<0.05.

group (DVDMS), SDT once for 2 weeks group (SDT1), and SDT once a week for 2 weeks group (SDT2) (Fig. 5A). There was no significant difference in body weight between the five groups in the observation period (Fig. 5B). Representative images of mice in each group at the end point are presented in Fig. 5C. Ultrasound alone (US) and DVDMS alone (DVDMS) resulted in some degree of anti-tumor activity. Anti-tumor activity became stronger when the number of times that DVDMS-SDT was applied was increased. Tumor weight and volume were significantly inhibited in the SDT2 group compared to the SDT1 and control groups (Fig. 5D–F).

Histopathological changes in mice

During the observation period, we did not observe obvious adverse effects, such as skin sensitivity or toxic death in the treated groups. After paraffin sectioning, the important organs and tumor tissues of the different groups were observed under a light microscope after H&E staining. The heart, liver, spleen, lung, and kidney from the different groups of mice did not reveal pathological changes (Fig. 6). Conversely, the tumor tissues were sparse and separated from each other in the SDT1 group compared to the control group. The structure of tumor tissue was more seriously damaged in the SDT2 group than in the SDT1 group and was accompanied by obvious vacant sections (Fig. 6).

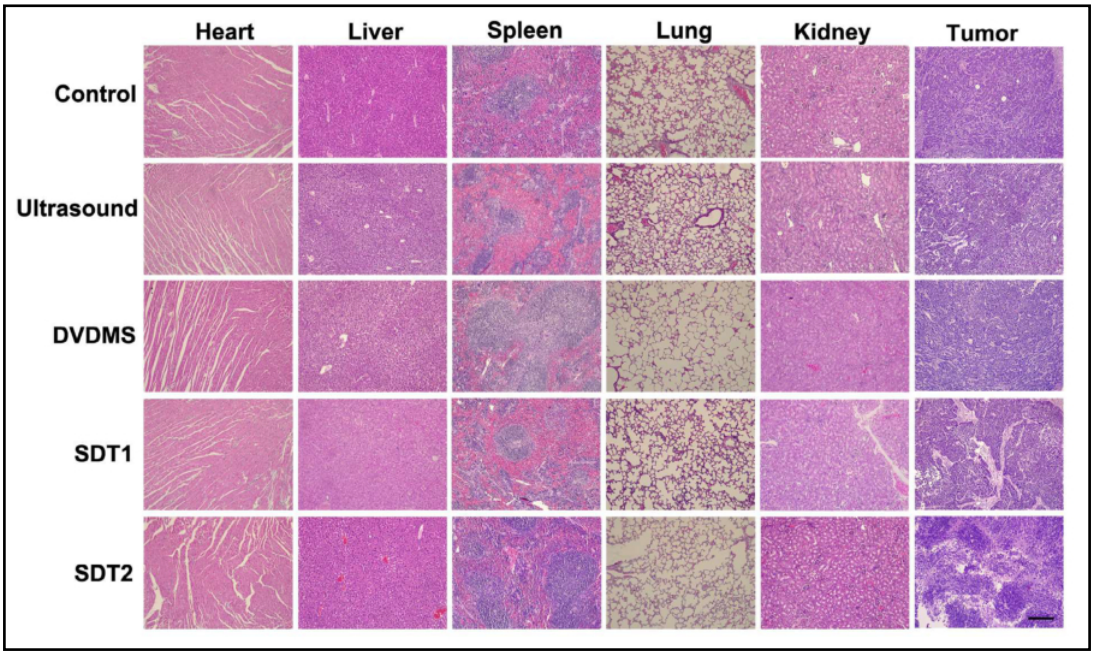

Fig. 6. Histopathological changes in mice. The heart, liver, spleen, lung, kidney, and tumor of different groups of mice at 15 days after treatment were stained by H&E. Scale bar represents 0.1 mm.

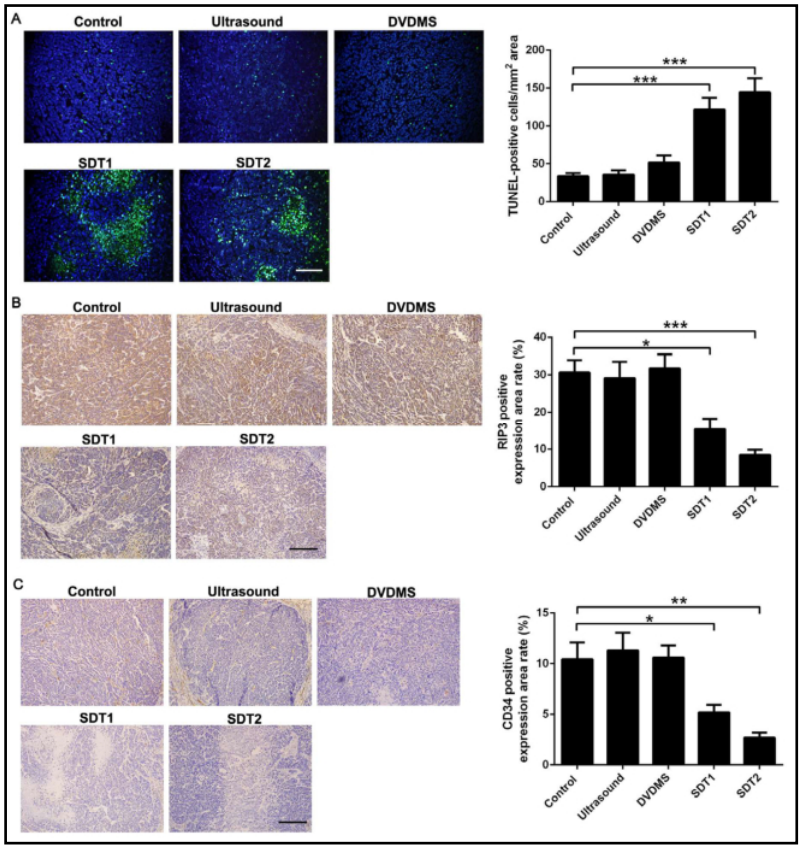

Fig. 7. DVDMS-SDT induces apoptosis and inhibits RIP3 and CD34 expression in vivo. (A) Representative images of TUNEL staining of apoptotic cells (green) in tumor tissue; nuclei (blue) were stained with DAPI. Scale bar represents 0.1 mm. Data shown represent the mean ± SD and were analyzed by ANOVA followed by the SNK test. ***P<0.001. (B) RIP3 expression in each group at 15 days after treatment. Scale bar represents 0.1 mm. Data shown represent the mean ± SD and were analyzed by ANOVA followed by the SNK test. *P<0.05, ***P<0.001. (C) CD34 expression in each group at 15 days after treatment. For expression analysis, 6 areas were selected randomly under a microscope. Data shown represent the mean ± SD and were analyzed by ANOVA followed by the SNK test. *P<0.05, **P<0.01.

TUNEL assays

TUNEL assays were used to detect whether apoptosis was induced by DVDMS-SDT *in vivo*. As show in Fig. 7A, US alone and DVDMS alone resulted in less apoptosis, as observed in the control group, whereas positive particles exhibiting green fluorescence (indicative of apoptosis) were significantly increased in the SDT groups. The apoptosis rate was increased according to the duration of SDT (SDT1 and SDT2 groups) and was at least 3- and 4-fold greater, respectively, than in the other groups. The data indicated that DVDMS-SDT could also induce apoptosis *in vivo*, thereby contributing to the suppression of tumor growth.

DVDMS-SDT inhibits RIP3 and CD34 expression in vivo

Due to the low level of VEGF expression in DVDMS-SDT, H446 cells were associated with decreased angiogenesis in our studies (Fig. 4). We further explored whether a similar phenomenon exists regarding CD34 expression in mouse tumor tissue. Anti-CD34 immunohistochemical analysis of tumor sections revealed that DVDMS-SDT significantly reduced microvessel density after treatment (Fig. 7C). SDT2, compared with SDT1, resulted in the enhanced inhibition of tumor vasculature, as indicated by CD34-positive endothelial cells (brown).

To investigate RIP3 expression *in vivo*, paraffin-embedded tumor tissue sections were examined by immunohistochemistry using an anti-RIP3 antibody. DVDMS-SDT decreased RIP3 expression in a treatment time-dependent manner, which was consistent with its inhibitory effects *in vitro* (Fig. 7B).

Discussion

Our results indicated that tumor growth was significantly inhibited by SDT with DVDMS, a novel sonosensitizer. Furthermore, the practical potential of DVDMS as a sonosensitizing drug was demonstrated by virtue of its properties such as high solubility in water and short period of skin sensitivity. This is the first study to provide evidence that RIP3 expression is inhibited by DVDMS-SDT in H446 cells, which indicates that necroptosis did not occur following DVDMS-SDT. We observed that the anti-tumor effect of DVDMS-SDT was generated through the apoptosis pathway with the involvement of ROS.

Previous studies have reported that different ultrasonic intensities combined with diverse sound-sensitive agents produce distinct biological effects on specialized cells and tissues [26-28]. In this study, we demonstrated that when DVDMS was used in conjunction with ultrasound (diameter: 3.5 cm; resonance frequency: 0.5 MHz; duty factor: 10%; repetition frequency: 100 Hz) on the SCLC H446 cell line, apoptosis was observed. Our findings are different to those reported by Hirotomo et al. [2]. They examined 16 separate cancer lines derived from seven types of cancer (lung, breast, pancreatic, stomach, liver, colon, and prostate). The researchers used the novel sensitizer DEG, which shows very little phototoxicity. They treated the cells using 1.0 MHz, 1.0 W/cm^2 output intensity, and a 10% duty cycle for 1–2 min. They found that cytotoxic effects after SDT with DEG mainly resulted in necrosis (unregulated cell death) associated with membrane lipid peroxidation, and not programmed cell death or apoptosis, both *in vitro* and *in vivo*. Under our experimental conditions, the number of apoptotic cells did increase after ultrasonic irradiation with DVDMS *in vitro*. A shift from apoptotic to necrotic cell death (detected using a particular dye) has been observed with increasing PDT intensity [29, 30]. The various parameters of ultrasound used in these studies may result in different types of cell death. The use of different sonosensitizers has played an important role in elucidating the mechanisms by which SDT causes cell death. During apoptosis, a cell undergoes programmed cell death in a controlled manner, whereas the necrotic mechanisms of cell death are more traumatic, resulting in large amounts of cell debris [31]. Necrosis and cell debris can be exploited to induce inflammatory immune responses, which aid tumor eradication and reduce metastatic disease [32]. Further experiments should be performed to clarify the details of the cell death

pathways induced by SDT.

Apoptosis is a form of programmed cell death that is essential for maintaining homeostasis, including the onset, progress, and resolution of immune reactions. Two major apoptosis pathways, i.e., extrinsic (mediated by death receptors) and intrinsic (mitochondrial), have been distinguished [33]. Mitochondria play an essential role in the induction of apoptosis by activating a variety of apoptosis-associated molecules that initiate the cascade of caspase activation [34]. Therefore, we performed a subsequent study to investigate changes of MMP in H446 cells exposed to DVDMS-SDT. We observed a loss of MMP in H446 cells following DVDMS-SDT. Next, we explored apoptosis-associated molecules and subsequent apoptotic events. Our results showed that DVDMS-SDT evidently increased the levels of c-caspase-3, c-caspase-8, c-caspase-9, and caspase-10, while the expression of BCL-2 protein, which is an anti-apoptotic protein in the mitochondrial apoptosis pathway [35], was decreased *in vitro*. These results indicated that DVDMS-SDT induced apoptosis in H446 cells via the mitochondrial caspase pathway, and caspase-8 and caspase-10 cleavage occurs, indicating that the extrinsic apoptosis is also involved.

ROS have been suggested to be one of the main effectors of SDT-induced apoptosis [36, 37]. In the present study, we provided evidence that DVDMS-SDT induced ROS generation. The level of ROS was increased with time after DVDMS-SDT, and reached a maximum at approximately 3–4 h, which was followed by a slow decline until 6 h. The free radical scavenger NAC prevented DVDMS-SDT-induced apoptosis and prevented changes to the expression of mitochondrial apoptosis-related proteins. However, it is interesting to note that the ultrasound intensities employed in this study did increase ROS levels, which may due to sonoluminescence via stable cavitation. These results demonstrated that reactive oxygen is the trigger for the mitochondrial apoptosis pathways induced by DVDMS-SDT.

RIP3 has emerged as a critical regulator of necroptosis, an inflammatory form of cell death with important functions in the development of cancer [38]. However, there is no clear evidence to indicate whether RIP3 is overexpressed following SDT. The present study, to our knowledge, is the first to confirm the expression of RIP3 in H446 cells exposed to DVDMS-SDT. Our results suggested that RIP3 expression was reduced by DVDMS-SDT *in vivo* and *in vitro*. In addition, pre-treatment with NAC almost completely restored RIP3 expression *in vitro*. Taken together, these findings lead us to conclude that the DVDMS-SDT-reduced expression of RIP3 was related to ROS generation, and RIP3 possibly plays a regulating role in necroptosis. However, there is no clear evidence to indicate whether necroptosis is inhibited by DVDMS-SDT. Further work is required to answer this important question and understand how we can harness the power of RIP3-dependent necroptosis in anti-cancer SDT.

The tumor microenvironment is essential for tumor growth and metastasis. In the tumor microenvironment, inflammatory cells and molecules influence almost every aspect of cancer progression [39]. VEGF is now accepted to play a major role in the continuous growth and metastasis of tumors [24]. Here, we found that DVDMS-SDT selectively down-regulated TNF-α and VEGF protein expression in H446 cells. Previous studies have shown that the combination of ultrasound with DVDMS decreased VEGF expression, which was consistent with its inhibitory effects on CD34 expression. In our study, we found that the decreased levels of VEGF and TNF-α could be significantly reversed by NAC. CD34 expression was reduced in xenograft tumor tissues by DVDMS-SDT in a treatment time-dependent manner. Taken together, it seems reasonable to conclude that DVDMS-SDT-induced ROS generation would exclusively be the trigger for the activation of mitochondrial apoptosis pathways, which initially alter the expression of TNF-α and VEGF.

In this study, DVDMS-SDT caused significant inhibition of tumor growth in a BALB/c nude mouse xenograft model. On the basis of the results of an *in vivo* toxicity study, DVDMS-SDT is safe at the tested dose. However, our evaluation of the safety of DVDMS-SDT was somewhat limited. Wang et al. reported that three treatments with ultrasound exposure at 2, 6, and 24 h after DVDMS injection to maximally excite DVDMS in tumor tissue produced much higher anti-tumor efficiency. In our study, we performed SDT treatment once for 2 weeks (SDT1) and SDT treatment once a week for 2 weeks (SDT2). We found that SDT2, compared

with SDT1, resulted in the enhanced inhibition of tumor weight, volume, and vasculature, as indicated by CD34-positive endothelial cells. TUNEL assays demonstrated that the apoptosis rate was significantly increased in the SDT2 group. These finding indicated that, to achieve lasting anti-tumor effects, multiple rounds of DVDMS-SDT are needed. Further experiments are necessary to optimize DVDMS-SDT to improve its efficacy.

In conclusion, we report strong evidence suggesting that DVDMS-SDT induces apoptosis in H446 cells *in vivo* and *in vitro*, in part by targeting the mitochondria through both the extrinsic and intrinsic apoptosis signaling pathways, and that apoptosis and the change in RIP3 expression are closely related to the generation of ROS. DVDMS-SDT showed efficient anti-cancer effects in an H446 nude mouse xenograft model, with no visible side effects. Our results strongly support the notion that SDT with DVDMS will be useful for the management of SCLC. This approach will be advantageous because it is noninvasive and can be applied repeatedly to patients.

Acknowledgements

This work was supported by the National Natural Science Foundation of China (81572824 and 81701848), Haiyan Foundation of Harbin Medical University Cancer Hospital (JJZD2016-01), and Innovation Science Foundation of Harbin Medical University (2016LCZX57, 2016LCZX79, and 2017LCZX83).

Disclosure Statement

The authors declare that there are no conflicts of interest.

References

1 Wang S, Tang J, Sun T, Zheng X, Li J, Sun H, Zhou X, Zhou C, Zhang H, Cheng Z, Ma H, Sun H: Survival changes in patients with small cell lung cancer and disparities between different sexes, socioeconomic statuses and ages. Sci Rep 2017;7:1339.

2 Tsuru H, Shibaguchi H, Kuroki M, Yamashita Y, Kuroki M: Tumor growth inhibition by sonodynamic therapy using a novel sonosensitizer. Free radical biology & medicine 2012;53:464-472.

3 Ahmed HU, Moore C, Emberton M: Minimally-invasive technologies in uro-oncology: The role of cryotherapy, hifu and photodynamic therapy in whole gland and focal therapy of localised prostate cancer. Surgical oncology 2009;18:219-232.

4 Cai XJ, Li WM, Zhang LY, Wang XW, Luo RC, Li LB: Photodynamic therapy for intractable bronchial lung cancer. Photodiagnosis and photodynamic therapy 2013;10:672-676.

5 Neuhaus J, Schastak S, Berndt M, Walther J, Dietel A, Sieger N, Stolzenburg JU: [photodynamic therapy of bladder cancer. A new option]. Der Urologe Ausg A 2013;52:1225-1232.

6 Story W, Sultan AA, Bottini G, Vaz F, Lee G, Hopper C: Strategies of airway management for head and neck photo-dynamic therapy. Lasers in surgery and medicine 2013;45:370-376.

7 Xiong W, Wang X, Hu J, Liu Y, Liu Q, Wang P: Comparative study of two kinds of repeated photodynamic therapy strategies in breast cancer by using a sensitizer, sinoporphyrin sodium. Journal of photochemistry and photobiology B, Biology 2016;160:299-305.

8 Xiong W, Wang P, Hu J, Jia Y, Wu L, Chen X, Liu Q, Wang X: A new sensitizer dvdms combined with multiple focused ultrasound treatments: An effective antitumor strategy. Scientific reports 2015;5:17485.

9 Costley D, Mc Ewan C, Fowley C, McHale AP, Atchison J, Nomikou N, Callan JF: Treating cancer with sonodynamic therapy: A review. International journal of hyperthermia : the official journal of European Society for Hyperthermic Oncology, North American Hyperthermia Group 2015;31:107-117.

10 Li C, Zhang K, Wang P, Hu J, Liu Q, Wang X: Sonodynamic antitumor effect of a novel sonosensitizer on s180 solid tumor. Biopharmaceutics & drug disposition 2014;35:50-59.

11 Liu Y, Wang P, Liu Q, Wang X: Sinoporphyrin sodium triggered sono-photodynamic effects on breast cancer both *in vitro* and *in vivo*. Ultrasonics sonochemistry 2016;31:437-448.
12 Wang H, Wang P, Li L, Zhang K, Wang X, Liu Q: Microbubbles enhance the antitumor effects of sinoporphyrin sodium mediated sonodynamic therapy both *in vitro* and *in vivo*. International journal of biological sciences 2015;11:1401-1409.
13 Wang X, Hu J, Wang P, Zhang S, Liu Y, Xiong W, Liu Q: Analysis of the *in vivo* and *in vitro* effects of photodynamic therapy on breast cancer by using a sensitizer, sinoporphyrin sodium. Theranostics 2015;5:772-786.
14 Yumita N, Okudaira K, Momose Y, Umemura S: Sonodynamically induced apoptosis and active oxygen generation by gallium-porphyrin complex, atx-70. Cancer Chemother Pharmacol 2010;66:1071-1078.
15 Hu J, Wang X, Zhang K, Wang P, Su X, Li Y, Huang Z, Liu Q: Sinoporphyrin sodium: A novel sensitizer in sonodynamic therapy. Anti-cancer drugs 2014;25:174-182.
16 Hu J, Wang X, Liu Q, Zhang K, Xiong W, Xu C, Wang P, Leung AW: Antitumor effect of sinoporphyrin sodium-mediated photodynamic therapy on human esophageal cancer eca-109 cells. Photochemistry and photobiology 2014;90:1404-1412.
17 Cui YL, Qiu LH, Zhou SY, Li LF, Qian ZZ, Liu XM, Zhang HL, Ren XB, Wang YQ: Necroptosis as a potential therapeutic target in multiple organ dysfunction syndrome. Oncotarget 2017;8:56980-56990.
18 Zhang YY, Liu H: Connections between various trigger factors and the rip1/ rip3 signaling pathway involved in necroptosis. Asian Pacific journal of cancer prevention : APJCP 2013;14:7069-7074.
19 Negroni A, Colantoni E, Pierdomenico M, Palone F, Costanzo M, Oliva S, Tiberti A, Cucchiara S, Stronati L: Rip3 and pmlkl promote necroptosis-induced inflammation and alter membrane permeability in intestinal epithelial cells. Digestive and liver disease : official journal of the Italian Society of Gastroenterology and the Italian Association for the Study of the Liver 2017;49:1201-1210.
20 Shi R, Li C, Jiang Z, Li W, Wang A, Wei J: Preclinical study of antineoplastic sinoporphyrin sodium-pdt via *in vitro* and *in vivo* models. Molecules 2017;22:E112.
21 You P, Wu H, Deng M, Peng J, Li F, Yang Y: Brevilin a induces apoptosis and autophagy of colon adenocarcinoma cell ct26 via mitochondrial pathway and pi3k/akt/mtor inactivation. Biomed Pharmacother 2017;98:619-625.
22 Bixel K, Saini U, Kumar Bid H, Fowler J, Riley M, Wanner R, Deepa Priya Dorayappan K, Rajendran S, Konishi I, Matsumura N, Cohn DE, Selvendiran K: Targeting stat3 by ho3867 induces apoptosis in ovarian clear cell carcinoma. International journal of cancer 2017;141:1856-1866.
23 Eriksson M, Pena-Martinez P, Ramakrishnan R, Chapellier M, Hogberg C, Glowacki G, Orsmark-Pietras C, Velasco-Hernandez T, Lazarevic VL, Juliusson G, Cammenga J, Mulloy JC, Richter J, Fioretos T, Ebert BL, Jaras M: Agonistic targeting of tlr1/tlr2 induces p38 mapk-dependent apoptosis and nfkappab-dependent differentiation of aml cells. Blood advances 2017;1:2046-2057.
24 Pan B, Shen J, Cao J, Zhou Y, Shang L, Jin S, Cao S, Che D, Liu F, Yu Y: Interleukin-17 promotes angiogenesis by stimulating vegf production of cancer cells via the stat3/giv signaling pathway in non-small-cell lung cancer. Sci Rep 2015;5:16053.
25 Wen SH, Lin LN, Wu HJ, Yu L, Lin L, Zhu LL, Li HY, Zhang HL, Li CC: Tnf-alpha increases staphylococcus aureus-induced death of human alveolar epithelial cell line a549 associated with rip3-mediated necroptosis. Life Sci 2018;195:81-86.
26 Wan GY, Liu Y, Chen BW, Liu YY, Wang YS, Zhang N: Recent advances of sonodynamic therapy in cancer treatment. Cancer biology & medicine 2016;13:325-338.
27 Dai ZJ, Li S, Gao J, Xu XN, Lu WF, Lin S, Wang XJ: Sonodynamic therapy (sdt): A novel treatment of cancer based on sonosensitizer liposome as a new drug carrier. Medical hypotheses 2013;80:300-302.
28 Li Q, Kang J, Xiong X, Liu Y, Cao W, Liu Y, Li Y: Protoporphyrin ix-mediated sonodynamic therapy promotes autophagy in vascular smooth muscle cells. OncolLett 2017;14:2097-2102.
29 Kharroubi Lakouas D, Huglo D, Mordon S, Vermandel M: Nuclear medicine for photodynamic therapy in cancer: Planning, monitoring and nuclear pdt. Photodiagnosis Photodyn Ther 2017;18:236-243.
30 Bharathiraja S, Manivasagan P, Santha Moorthy M, Bui NQ, Jang B, Phan TTV, Jung WK, Kim YM, Lee KD, Oh J: Photo-based pdt/ptt dual model killing and imaging of cancer cells using phycocyanin-polypyrrole nanoparticles. Eur J Pharm Biopharm 2018;123:20-30.

31 Ren Y, Gallucci JC, Li X, Chen L, Yu J, Kinghorn AD: Crystal structures and human leukemia cell apoptosis inducible activities of parthenolide analogues isolated from piptocoma rufescens. J Nat Prod 2018;81:554-561.
32 Pizova K, Tomankova K, Daskova A, Binder S, Bajgar R, Kolarova H: Photodynamic therapy for enhancing antitumour immunity. Biomedical papers of the Medical Faculty of the University Palacky, Olomouc, Czechoslovakia 2012;156:93-102.
33 Alves ACS, Dias RA, Kagami LP, das Neves GM, Torres FC, Eifler-Lima VL, Carvalho I, de Miranda Silva C, Kawano DF: Beyond the "lock and key" paradigm: Targeting lipid rafts to induce the selective apoptosis of cancer cells. Curr Med Chem 2018;25:2082-2104.
34 Kim SH, Kim KY, Park SG, Yu SN, Kim YW, Nam HW, An HH, Kim YW, Ahn SC: Mitochondrial ros activates erk/autophagy pathway as a protected mechanism against deoxypodophyllotoxin-induced apoptosis. Oncotarget 2017;8:111581-111596.
35 Russo A, Cardile V, Graziano ACE, Avola R, Bruno M, Rigano D: Involvement of bax and bcl-2 in induction of apoptosis by essential oils of three lebanese salvia species in human prostate cancer cells. Int J Mol Sci 2018;19:292.
36 McEwan C, Owen J, Stride E, Fowley C, Nesbitt H, Cochrane D, Coussios CC, Borden M, Nomikou N, McHale AP, Callan JF: Oxygen carrying microbubbles for enhanced sonodynamic therapy of hypoxic tumours. J Control Release 2015;203:51-56.
37 Su X, Wang P, Wang X, Guo L, Li S, Liu Q: Involvement of mapk activation and ros generation in human leukemia u937 cells undergoing apoptosis in response to sonodynamic therapy. International journal of radiation biology 2013;89:915-927.
38 Omoto S, Guo H, Talekar GR, Roback L, Kaiser WJ, Mocarski ES: Suppression of rip3-dependent necroptosis by human cytomegalovirus. J Biol Chem 2015;290:11635-11648.
39 Abadjian MZ, Edwards WB, Anderson CJ: Imaging the tumor microenvironment. Adv Exp Med Biol 2017;1036:229-257.